Arabian Journal of Chemistry (2020) **13**, 7482–7489

King Saud University

Arabian Journal of Chemistry

www.ksu.edu.sa
www.sciencedirect.com

ORIGINAL ARTICLE

Two Co(II)-based metal-organic frameworks: Catalytic Knoevenagel condensation reactions and inhibitory activity on the scar tissue hyperplasia by reducing the activity of the VEGF signaling pathway

Jia-Bin Deng, Xin Wang, Zi-Qiao Ni, Fei Zhu *

Plastic Surgery, First Affiliated Hospital of Anhui Medical University, Hefei, Anhui, China

Received 6 July 2020; accepted 23 August 2020
Available online 29 August 2020

KEYWORDS

MOF;
Knoevenagel condensation;
Heterogeneous catalyst;
Scar tissue hyperplasia

Abstract In the current research, two porous Co(II)-containing metal–organic frameworks (MOFs) with chemical formulae can be teamed as $[Co_2(bptc)(H_2O)_2]\cdot 5DMA$ (**1**, H_4bptc = biphenyl-3,3′,5,5′-tetracarboxylic acid) and $[Co_2(Hatta)_2\cdot(H_2O)_3]\cdot 3DMA$ (**2**, H_4atta = 2′-amino-[1,1′:4′,1″-terphenyl]-3,3″,5,5″- tetracarboxylic acid) have been solvothermally synthesized by using two similar tetracarboxylic ligands and structurally characterized. The complex **2** with amino-functionalized pores could be used as recoverable heterogeneous catalytic agent for Knoevenagel condensation without solvents. The inhibitory activity of compounds on the scar tissue hyperplasia was evaluated and the related mechanism was discussed as well. First of all, the proliferation of the human hypertrophic scar fibroblasts was measured after indicated treatment was measured by CCK-8 assay. Next, the real time RT-PCR was applied to determine the activation power of the VEGF signaling pathway after using compounds.

1. Introduction

Hypertrophic scars are an important clinical problem after trauma, burns and plastic surgery. They are caused by abnormal fibrosis of tissues during wound healing due to the imbalance of tissue repair and regeneration mechanisms, which can cause lasting loss of function and shape damage (Ogawa, 2017; Lee and Jang, 2018). The mechanism of hypertrophic scar formation has not been elucidated, and there is no particularly effective treatment method up to now. The expression of

* Corresponding author.
E-mail address: fei_zhu66@yeah.net (F. Zhu).
Peer review under responsibility of King Saud University.

ELSEVIER Production and hosting by Elsevier

https://doi.org/10.1016/j.arabjc.2020.08.023
1878-5352

COX-2 and VEGF is related to the mechanism of scar tissue formation (Agarwal et al., 2017). COX-2 may promote scar hyperplasia by inducing angiogenesis, and the VEGF could directly stimulate the proliferation of the human hypertrophic scar fibroblasts.

The crystalline material teamed as metal-organic frameworks (MOFs) have many advantages, such as persistent porosity, variety of species and structure controllability. It has potential application value in the field of gas separation, sensor industry and photoelectron chemical industry, so it is one of the most eye-catching crystal materials (Paul et al., 2020; Adonin et al., 2020; Andrusenko et al., 2016; Il'in et al., 2017; Dhakshinamoorthy et al., 2017; Das et al., 2019). At the same time, the synthesis of MOFs with strong functionality and diversity is the focus of current research. However, the framework of MOFs is affected by numerous factors, such as different coordination modes, metal species, chemical reaction environment, etc., which makes it difficult to obtain the designed MOFs in practice (Burgoyne and Meijboom, 2013; Opanasenko et al., 2013; Das et al., 2019). The common way to synthesize target MOFs is to combine the characteristic secondary building unit (SBU) with the designed connector, which is universal and efficient, and provides a platform to realize the value of materials carrying the required functions (Dhakshinamoorthy et al., 2013; Feng et al., 2019, 2017; Zhang et al., 2020; Du et al., 2018). Among all organic ligands, inflexible dicarboxylic acids are widely used to form new MOFs because of their excellent capability of coordination and various coordination modes. Furthermore, the tetracarboxylic ligands with the isophthalic acid coordination donors have been largely applied to construct the porous MOFs with cage or channel-type framework (Fu et al., 20; Qian et al., 2017; Du et al., 2018; Wang et 2018; et al., 2020). Taking into account the abo acte in the research, two porous Co(II)-containing -organ frameworks (MOFs) with the chemical form of $(H_2O)_2]\cdot 5DMA$ (**1**, H_4bptc = enyl ,5′-tetracarboxylic acid) and $[Co_2(Hatta)_2\cdot(H_2O)_3]\cdot 3DMA$ (H_4atta = 2′-amino-[1,1′:4′,1″-terphenyl]- , tetracarbo c acid) have been solvothermally synthesized using two similar tetracarboxylic ligands structurally characterized. The complex **2** with amin nctionalized pore ould be used as recoverable hetero eous catalytic agent for Knoevenagel condensation witho s. After serious experiment, the inhibition of compound s deter ed and the internal principles was at the e. The data of the CCK-8 assay s ested t compo **1** had a more powerful inhibition a y in to compound **2** on the proliferation of the huma rtrop car fibroblasts. In addition to this, the promot evel of the VEGF signaling pathway was also substantially ced under compound **1** treatment, compound with compound **2**, which was proved by the real time RT-PCR experiment.

2. Experimental

2.1. Chemicals and measurements

The whole materials in the experiment were obtained from the markets and used without deeper refine. In order to record the KBr pellets ranges 400–4000 cm^{-1}, we used the Nexus 870 FTIR spectrometer to scan the samples. Elemental analyses (EA) were operated by applying a PerkinElmer 240 elemental analyzer. ^1H NMR spectra were reported on the Bruker DRX spectrometer (400 MHz) in CDCl3.

2.2. Preparation and characterization for $[Co_2(bptc)(H_2O)_2]\cdot 5DMA$ (1) and $[Co_2(Hatta)_2\cdot(H_2O)_3]\cdot 3DMA$ (2)

Complex **1** is formed by mixing 120 mg $Co(NO_3)_3\cdot 6H_2O$, 33 mg H_4bptc, 0.2 mL HNO_3(65 wt%),3.0 mL 1,4-dioxane and 3.0 mL *N*,*N*-dimethylacetamide (fter stirring, the mixture was set in a 20 mL vital heated ighty five degrees last for 120 h. After lowe to the norm environment, pink chunk-shaped cr tals re obtai in *ca.* 58% yield. All crystals ar st filtere en ned with DMA to detach irreleva y-pro cts, a ly dried to obtain. Anal. Cald. F the bon conte t is 49.38; the hydrogen content is 96; nitroge ntent is 12.52 percent. Found: the bon con s 49. he hydrogen content is 4.93, the ni content is

Comple is d by mixi 0.0105 g H_4atta, 0.0291 g $Co(NO_3)_2\cdot 6H_2O$ and L DMA-methanol-H_2O (the rate is: 5/2/1 stirring fo f an hour**, 2** was set in a 20 mL Te container and hea ed at eighty five degrees last for o day. After l ering to the normal environment, crystals **2** e obtained 62.3% yield. All crystals are first filtered, the shed w DMA to detach irrelevant by-products, and fi to obtain. Elemental analysis for **2**: the carbon content is 42.90; the hydrogen content is 5.36; and the content is 7.36 percent. Found: the carbon content 42.78, the hydrogen content is 5.39, the nitrogen content is 7.07.

In order to obtain the data of X-ray, we use the Oxford Xcalibur E diffractometer. Statistical analysis of various strength data was performed using crysalispro software and the results were converted to HKL format. The pattern of SHELXS based on direct means was applied for establishing the primary framework patterns, and the pattern of SHELXL-2014 based on least square method was altered. The atom except hydrogen atom is refined by using different heterogenous parameters. Next, the whole of H atoms with applying AFIX program to fasten on the C atom. Table S1 displays the details and data of complex **1** and **2**.

2.3. Human hypertrophic scar fibroblasts proliferation

The Cell Counting Kit-8 was operated to measure the proliferation of the human hypertrophic scar fibroblasts after compounds treatment. This preformation was operated under the illustration of the manufacturers with some changes. In a word, the human hypertrophic scar fibroblasts in the coherent growing phage were gathered and cultivated into the tissue cultivate plates at the ultimate destiny of 10^4 cells per well. Next, the cells were cultivated with compound **1** or **2** at different concentrations. After that, the cells were dyed by the CCK-8 reagent and the absorbance of every well was evaluated by flow cytometry. The experiment was operated greater than or equal to 3 times, and the data were recorded as mean ± SD.

2.4. VEGF signaling pathway activation

Next, the promotion ability of the VEGF signaling routine in the human hypertrophic scar fibroblasts was assessed through the real time RT-PCR assay. This conduction was finished in consistent with the manufactures' protocols with some changes. In a word, the human hypertrophic scar fibroblasts in the coherent growing phage were gathered and cultivated into the tissue cultivate plates at the ultimate destiny of 10^5 cells per well. Then, the cells were cultivated with compound **1** or **2** at indicated concentrations. All the cells were harvested, washed for the total RNA extraction with TRIZOL reagent. Next, the quantity of the whole RNA was measured, and then inverted transferred to the cDNA. Finally, the real time RT-PCR was operated for the *vegf* expression measurement, using the *gapdh* to the internal comparison. The $C^{-\Delta\Delta ct}$ method was used for the statistical analysis.

3. Results and discussion

3.1. Molecular structures

Complex **1** is formed by mixing $Co(NO_3)_3{\cdot}6H_2O$, H_4bptc, DMA, 1,4-dioxane and a little HNO_3. After stirring, the mixture was heated at eighty five degrees last for 120 h. After lowering to the normal environment, crystalline products of **1** were obtained. In order to determine the purity of compound **1**, element analysis (EA) was used to detect it. According to the experimental data of single crystal X-ray diffraction, 1 lized in the triangular space group *R-3 m*. The lattice pa ne- ters of *a* and *b* are 18.5540(8) Å, 24.731(2) Å for *c*, 90° α and *β* , 120° for *γ*. The asymmetric part is f separa Co(ii) ion, and one fourth of $bptc^{4-}$ ligand f the t minal coordination water molecules in th axial sit (Fig. 1a). The central Co(ii) ions are rdin carboxyl oxygen atoms of variou ptc^{4-} s and a half oxygen atom of coordination w molecule, ming a trigonal bipyramidal configurati bptc^{4-} liga displays a $(\kappa^1\text{-}\kappa^1)\text{-}(\kappa^1\text{-}\kappa^1)\text{-}(\kappa^1\text{-}\kappa^1)\text{-}(\kappa^1\text{-}\kappa$ μ_8 c ination pattarn and double Co(ii) ions are nected by f bridging carboxylate produce the $Co_2(CO$ impeller SBUs 1b). Compound **1**, similar to MO 05 an OTT-100 compounds, is composed of two kin f al ative filling open coops. Six $Co_2(COO)_4$ impeller SB e conn d with 12 $bptc^{4-}$ ligands, and the of S ar out 9 Å, then eight octahedrons asse led to a cubic octahedral coop with an ical c which cage is about 14 × 8 Å^2 (Fig. 1c). Two ges are arranged alternately by using triangula d quadrilateral windows to form a three-dimensiona e stacking frame with two different types of one-dimensio paths (about 7.5 Å in diameter) along the c-axis (Fig. 1d). Calculated accessible pore volume of **1** is as high as 64.0%.

Complex **2** were obtained by mixing $Co(NO_3)_2{\cdot}6H_2O$ with H_4atta (2′-amino-[1,1′:4′,1′′-terphenyl]-3,3′′,5,5′′-tetracarboxylic acid) ligand in DMA-Methanol-H_2O mixed solvent at 85 °C for 24 h. According to the single crystal results gathered at natural temperature and the analysis of its structure, the results reveal that the complex **1** is a three-dimensional structure formed crystals in the $P2_1$ group, where is a monoclinic space. Fig. S1a shows that there are two types of coordination modes for Co^{2+} ions. Co1 consists of four O atoms from chelated carboxylic acid group and two O atoms from monodentate coordinated carboxylic acid group to form six coordination mode. Co2 consists of three O atoms from different coordination water molecules and three O atoms from monodentate coordinated carboxylic acid group to form six coordination mode. The bond length range of Co-O is 1.995(6) Å to 2.084(6) Å, which is similar to that of other Co(II)-MOFs based on tetracarboxylic acid ligands. The four carboxylic groups in the Hatta$^-$ ligand show three different types of coordination patterns that are μ1-(η1: η1), μ2-(η1: η1) and μ2-(η2: η1), which links wi contiguous Co (II) ions (Fig. S1b). The formed $_2O_6\}$ ers are connected by the tetragonal organic nds to co ct a three-dimensional structure with two kin one-dime onal paths along the a-axis and c-axis ich are with free –NH_2 groups (Fig. S1c and Fi 1d). The solv ssible volume of **2** after the remova the c inated a lattice guests is 1655 Å^3, which ac ou .3% of e crystal volume.

To check th hase p of the oducts, powder X-ray diffraction (P D) experi e been carried out for these com te g. S2, Supp ng Information). The peak positions of the e imental and simulated PXRD patterns are i d agreeme with each other, indicating that the c al structures are t y representative of the bulk crystal oducts. The differences in intensity may be owing to the pre- red orienta n of the crystal samples. To characterize the p ity of c plexes **1** and **2**, N_2 adsorption experiments we f d at 77 K. Before the gas sorption experiments, about 100 mg of the as-prepared two complexes were soaked in Cl$_2$ for three days, and then the solvent-exchanged samples were heated under the dynamic vacuum for 12 h to get the activated samples of **1** and **2** (denoted as **1a** and **2a** hereafter). For **1a**, very low N_2 gas uptakes were found in **1a**, which may be explained as the partial collapse of the activated frameworks. This phenomenon is common for porous frameworks based on the similar paddle-wheel clusters (Chen and Zhang, 2019; Wang et al., 2015). The complex **2a** exhibited an N_2-uptake value of 204.9 cm^3/g at 1 atm, corresponding to a BET surface area of 764.5 m^2/g (Langmuir surface area of 817.2 m^2/g) and pore volume of 0.32 cm^3/g (Fig. 2a). According to Horvath-Kawazoe equation, the calculation based on N_2 desorption isotherm was carried out to reveal that main pore size focused on the scope of 0.6 to 0.7 nm, which completely coincided with the channel of crystal structure (Fig. 2a inset).

3.2. Catalytic experiment

Complex **2** has many excellent properties, such as rigid structure, large aperture, easy combination of –NH_2 groups and strong thermal stability. Therefore, it provides favorable conditions for the alkali catalytic reactions. Also, the Knoevenagel condensation of benzaldehyde derivatives with malononitrile was catalyzed by complex **2** as heterogeneous catalyst. Before being used as a catalyst, complex **2** was sensitized by exchanging and removing guest molecules from the channel. The activation of samples (**2a**) involves the following characteristic steps: 1 mmol of benzaldehyde derivatives, 2 mmol of malononitrile and 0.02 mmol of catalyst (**2a**) are put into a 10 mL round bottom flask and stirred at sixty degrees without

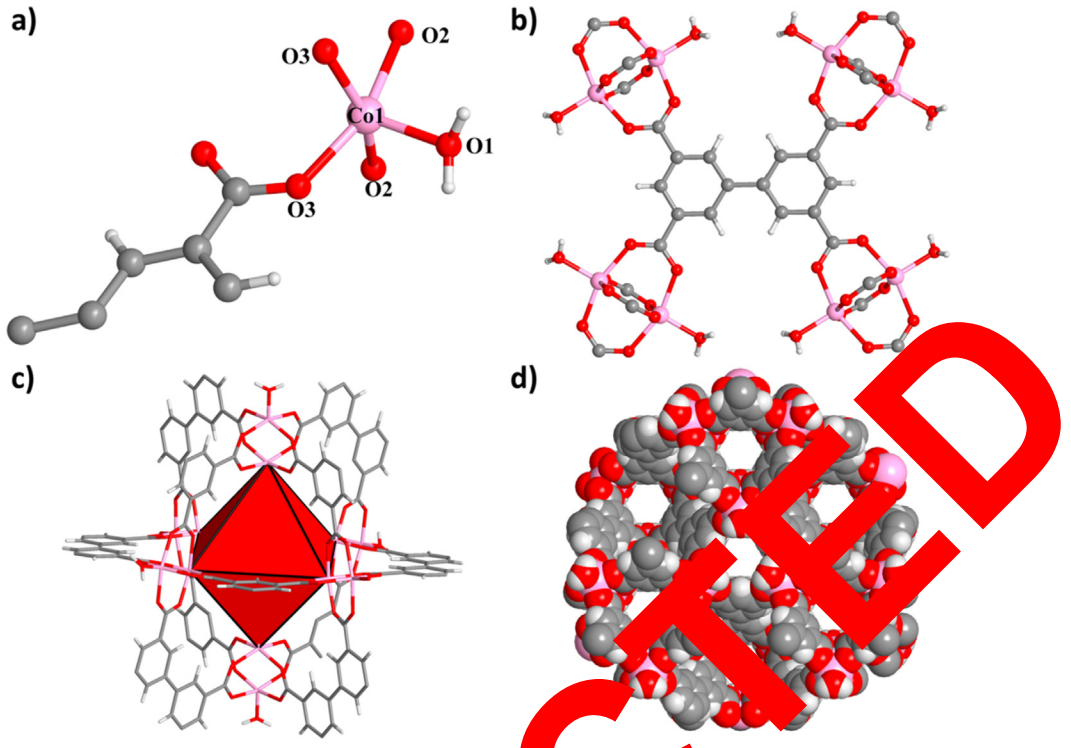

Fig. 1 (a) Image for the asymmetry part of **1**. (b) Image for the coordina[illegible] pattern of [illegible] $bptc^{4-}$ ligand. (c) The octahedral cage of **1**. (d) The three-dimensional structure of **1** displaying the one-dimensional path[illegible]

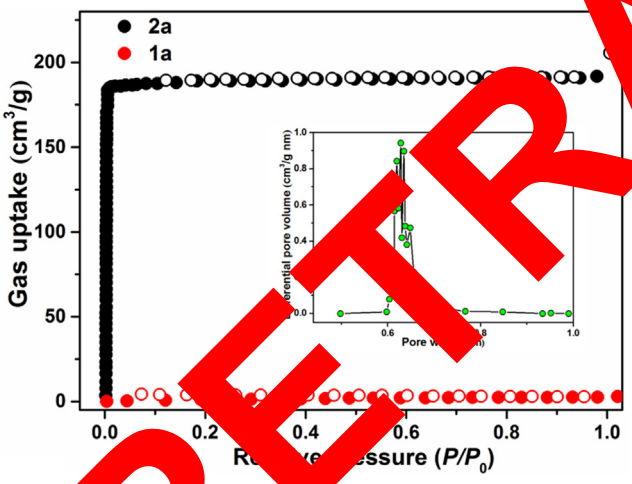

Fig. 2 [illegible] N_2 [illegible]otion profiles of 1a and 2a at 77 K. The inset shows th[illegible] [illegible]ions of **2a**.

solvent. The re[illegible]on procedure was observed by thin layer chromatography (TLC). The conversion of the reaction can be straightly measured by gas chromatography. As for benzaldehyde, the correlation between conversion and reaction time was investigated. Fig. 2 shows that with the increase of reaction time, the conversion rate of the reaction increases gradually, and the chemical reaction is completed within six hours, suggesting that **2a** can efficiently catalyze Knoevenagel condensation of benzaldehyde with malononitrile. Therefore, when benzaldehyde derivatives are used in Knoevenagel reaction, the reaction time is basically within six hours. In addition, [illegible]ain an insight of the catalyst role of **2a** in the reaction, a [illegible]ntrol experiment in the absence of catalyst was carried [illegible]ut under a similar reaction condition. As shown in the Fig. 3 the red points, almost catalytic activity can be observed even after 6 h, which highlights the catalyst role of **2a**. When using the $Co_2(NO_3)\cdot 6H_2O$ as the catalyst, only less than 10% conversion could be detected after 6 h. To prove the importance of the catalyst, the reaction stopped immediately after removing the catalysis **2a**, and no further conversion could be after 6 h, indicating the heterogeneous catalyst nature of **2a**. Mean-

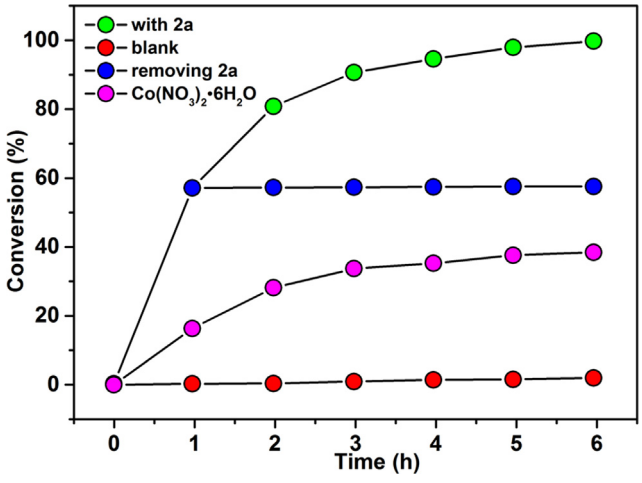

Fig. 3 Reaction conversion versus reaction time for Knoevenagel condensation of malononitrile and benzaldehyde with **2a** as catalyst.

while, the leaking of the Co(II) ion in the solution could be ruled out via the inductively coupled plasma massspectrometry (ICP-MS) analysis, which showed that the concentration of Co (II) ion is only 3.2 mg/L after one hour's reaction.

In order to detect the influence of substituents, various alternative benzaldehyde derivatives were used in the above experiments. Table 1 shows that the properties of substituents on the benzene ring significantly affect Knoevenagel condensation. The electron withdrawing group (–Br, –CN, $–NO_2$) is helpful to increase the conversion (yield > 99%, entries 4–7), while the electron donor group ($–OCH_3$, $–CH_3$) was not conducive to the conversion of the reaction, and the electron donor capacity was inversely related to the reaction yield (for $–CH_3$, the yield < 90%, for $–OCH_3$, the yield < 70%, entries 2 and 3). The different positions of substituents on benzene ring significantly affect Knoevenagel condensation reaction. The yields of benzaldehyde with electron withdrawing groups (–Br, –CN, $–NO_2$) at *ortho*- or *para*-site are significantly higher (entries 4–7), while those with electron donating groups ($–OCH_3$, $–CH_3$) are relatively low (entries 2 and 3). Moreover, the substituents located in the *ortho*- or *para*-site of aldehyde group have more influence on the substituents than that located in the *meta*-site. In contrast to *para*-site, the $–OCH_3$ in the *meta*-site of aldehyde group is favorable for the reaction (entries 3 and 8). This [illegible] due to the fact that $–OCH_3$ in the middle of the be[illegible]e ring [illegible]bits electron

Table 1 Knoevenagel condensation reactions of different benzaldehyde derivatives catalyzed [illegible] **2a**.

Entry	Substrate	Yield (%)
1	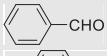	99.8
2		86
3	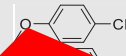	71
4		99.9
5		99.8
6		99.9
7		99.9
8	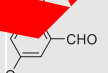	97
9	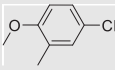	65
10	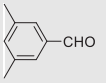	68

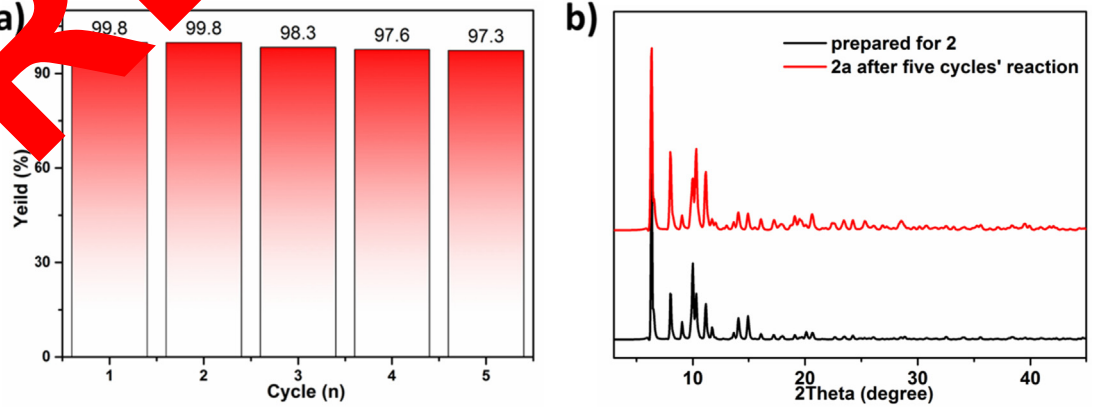

Fig. 4 The recycling tests for **2a**. (b) The PXRD patterns for **2** before and after five cycles' catalytic reaction.

absorption properties for the all benzaldehyde system, which makes the intermediate aldehyde group show stronger reaction activity. At the same time, the number of substituents on benzene has some influence on Knoevenagel condensation. With the increase of the quantity of electron donating groups on benzaldehyde, the yield of the reaction decreased gradually (entries 9 and 10).

In the end, in order to verify the recovery and stability of **2a**, the catalyst was reused for 5 times in catalytic reactions. The catalyst can be separated with no difficulty by centrifugation and recycled in a new catalytic experiment. After five catalytic experiments, the conversion rate did not decrease significantly (Fig. 4a). At the same time, the catalyst was characterized before and after five catalytic experiments. Fig. 4b indicates that the PXRD patterns of **2a** hardly change before and after the catalytic reaction, suggesting that they have great chemical stabilities. Thus, **2a** are stable and reusable heterogeneous catalyst for Knoevenagel condensation. As far as we know, only a few MOFs have been regarded as highly effective catalysts for Knoevenagel condensation in the present of solvent-free conditions.

4. Compound inhibited the proliferation of the human hypertrophic scar fibroblasts

After the synthesizing of compound **1** as well as compound **2**, their treatment activity on the wound healing and microshaping was evaluated. Thus in this present research, the CCK-8 report was firstly operated for the assessing of the inhibitory activity on the human hypertrophic scar fibroblasts. Fig. 5 suggests that comparing with the control model, compound **1** could markedly reduce the proliferation ability of the human hypertrophic scar fibroblasts; however, compound **2** had a little effect on the cell proliferation.

4.1. Compound reduced the activation level of the VEGF signaling pathway

In the above experiment, we have proved that compound **1** showed noteworthy inhibition on the human hypertrophic scar fibroblasts proliferation. However, the detail mechanism under this inhibition was still unclear. As the VEGF signaling pathway plays vital important role in the cell growth and proliferation, we next operated the real time RT-PCR to measure the activation level of the VEGF signaling routine after using compounds. From the data in Fig. 6, comparing with the control model, the promotion ability of the VEGF signaling pathway was obviously reduced after compounds treatment, which was consistence with the previous studies.

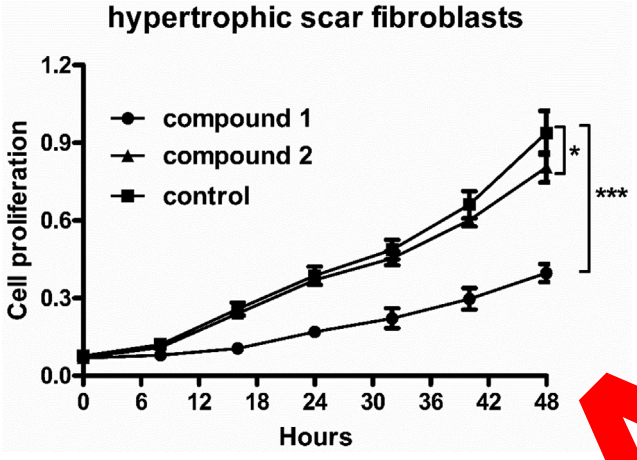

Fig. 5 Inhibited proliferation of the human hypertrophic scar fibroblasts after compound treatment. The human hypertrophic scar fibroblasts were dealt with compound **1** or **2** at the content of five milligram per kilogram. The production of the determined by CCK-8 assay.

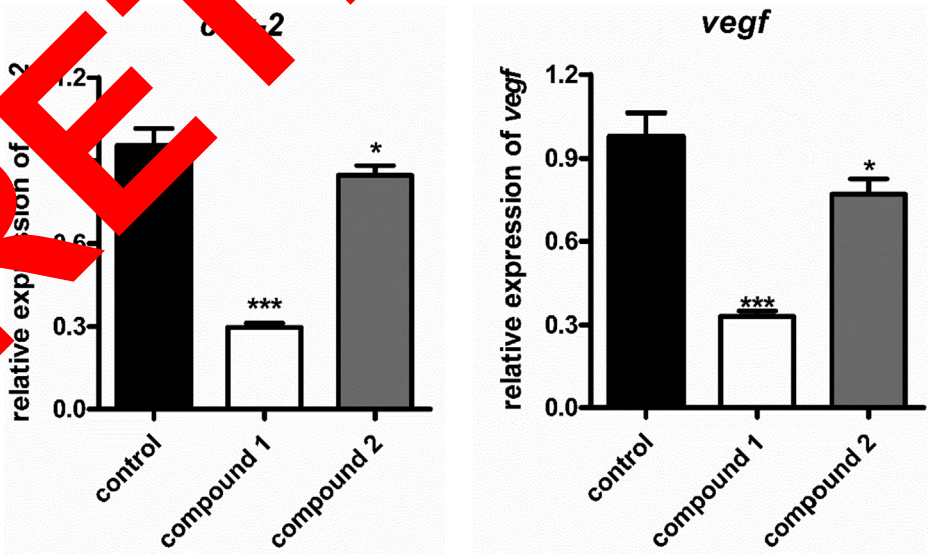

Fig. 6 Declined activation level of the VEGF signaling routine after using compounds. The human hypertrophic scar fibroblasts were dealt with compound **1** or **2** at the content of five mg/kg. The real time RT-PCR was operated to evaluate the promotion ability of the VEGF signaling pathway in the human hypertrophic scar fibroblasts.

5. Conclusion

In a word, we have constructed two porous Co(II)-including MOFs through using two similar tetracarboxylic ligands. The single crystal X-ray diffraction experiment suggests that complex **1** displays a three-dimensional cage-stacking structure with octahedral coops, cuboctahedral coops and two types of one-dimensional channel along the c-axis, and complex **2** shows 3D structure with two kinds of one-dimensional channels along the a-axis and c-axis which are decorated free amino groups. The complex **2** with amino-functionalized pores could be used as reusable heterogeneous catalyst for Knoevenagel condensation in the present of solvent-free conditions. From the CCK-8 assay, we can see that compound **1** had a significant inhibition on the human hypertrophic scar fibroblasts proliferation, but not compound **2**. Furthermore, through real time RT-PCR assay, we also showed that compound **1** had a more powerful inhibition than compound **2** on promotion level of the VEGF signaling routine. In conclusion, compound **1** was more excellent candidate for the wounds healing after micro-shaping.

6. Data Availability

The data used to support the findings of this study are included within the article.

Declaration of Competing Interest

The authors declare that they have no known com financial interests or personal relationships that could ve appeared to influence the work reported in this paper.

Acknowledgments

The research was foundered by Researc nd tute of Translational Medicine 7zhy and National Natural Science Foundation o na (3097

Appendix A. Supplement ry materia

Supplementary d to thi rticle can be found online at https://doi.org/ 16/j bjc.2020.08.023.

Referen

Ad S.A. ko, M.A., Novikov, A.S., Sokolov, M.N., 202 n isostructural Co(II) complexes with 2-halopy s. Crystals 10, 289.

Agarwal, S. in, M., Levi, B., 2017. Heterotopic ossification and hypertrophic ars. Clin. Plast. Surg. 44, 749–755.

Andrusenko, E.V., Novikov, A.S., Starova, G.L., Bokach, N.A., 2016. Three-dimensional hydrogen bonding network in the structures of (dimethylcyanamide)cobalt(II) complexes. Inorg. Chim. Acta 447, 142–149.

Burgoyne, A.R., Meijboom, R., 2013. Knoevenagel condensation reactions catalysed by metal-organic frameworks. Catal. Lett. 143, 563–571.

Chen, D.M., Zhang, X.J, 2019. Stepwise and hysteretic sorption of CO_2 in polycatenated metal-organic frameworks. CrystEngComm 21, 4696–4700.

Das, A., Anbu, N., Dhakshinamoorthy, A., Biswas, S., 2019. A highly catalytically active Hf(IV) metal-organic framework for Knoevenagel condensation. Micropor. Mesopor. Mat. 284, 459–467.

Das, A., Anbu, N., SK, M., Dhakshinamoorthy, A., Biswas, S., 2019. A functionalized UiO-66 MOF for turn-on fluorescence sensing of superoxide in water and efficient catalysis for Knoevenagel condensation. Dalt. Trans. 48, 17371–17380.

Dhakshinamoorthy, A., Opanasenko, M., Čejka, J., Garcia, H., 2013. Metal organic frameworks as solid catalysts in condensation reactions of carbonyl groups. Adv. Synth. Catal. 355, 247–268.

Dhakshinamoorthy, A., Heidenreich, N., Lenzen, D., Stock, N., 2017. Knoevenagel condensation reaction ca by Al-MOFs with CAU-1 and CAU-10-type structures ystE mm 19, 4187–4193.

Du, H., Ma, C., Ma, W., Wang, H., Microstru e evolution and dielectric properties of dope i4Ti4O1 ramics synthesized via glycine-nitrat cess. Proc ppl ram. 12, 303–312.

Du, J.L., Zhang, X.Y., P., G .P., Hou, J ., Jing, X., Mu, Y. J., Li, L.J., 201 A nal lum scent Zn(II)-MOF for detection of aroma xplosiv nd Fe^{3+} ions. Sensor. Actuat. B 257, 207–2

Feng, X., G en, H.P., W H.L., Yue, L.Y., Chen, X., Ng, S.W., X.F., L.F., Wang, L.Y., 2017. A series of anionic host-coordination p ers, based on azoxybenzene carboxylate: es, luminescen d magnetic properties. Dalton T. 46, 14192–14200.

g, X., Sha Y., Zhang, H., Li, R., Wang, W., Zhang, D., Wang, L., Z., 2019. Enhance luminescence and tuning gnetic p rties of lanthanide coordination polymers based ubstituted and phenanthroline ligands. RSC Adv. 9, 16328–16338.

H., Wang, M., Li, P., Jiang, S., Hu, W., Guo, X., Cao, M., 2019. ing knowledge development trajectories of the internet of things domain: a main path analysis. IEEE Trans. Ind. Inform. 15, 6531–6540.

Il'in, M.V., Bolotin, D.S., Novikov, A.S., Suslonov, V.V., Chezhina, N.V., Bubnov, M.P., Cherkasov, V.K., Venter, G.J.S., Roodt, A., 2017. Square-planar aminonitronate transition metal complexes (M = CuII, NiII, PdII, and PtII). Inorg. Chim. Acta 467, 372–378.

Lee, H.J., Jang, Y.J., 2018. Recent understandings of biology, prophylaxis and treatment strategies for hypertrophic scars and keloids. Int. J. Mol. Sci. 19, 711.

Li, Q., Qian, J., Du, L., Zhao, Q., 2020. Zinc-tetracarboxylate framework material with nano-cages and one-dimensional channels for excellent selective and effective adsorption of methyl blue dye. RSC Adv. 10, 3539–3543.

Ogawa, R., 2017. Keloid and hypertrophic scars are the result of chronic inflammation in the reticular dermis. Int. J. Mol. Sci. 18, 606.

Opanasenko, M., Dhakshinamoorthy, A., Shamzhy, M., Nachtigall, P., Horáček, M., Garcia, H., Čejka, J., 2013. Comparison of the catalytic activity of MOFs and zeolites in Knoevenagel condensation. Catal. Sci. Technol. 3, 500–507.

Paul, A., Martins, L.M.D.R.S., Karmakar, A., Kuznetsov, M.L., Novikov, A.S., Guedes da Silva, M.F.C., Pombeiro, A.J.L., 2020. Environmentally benign benzyl alcohol oxidation and C-C coupling catalysed by amide functionalized 3D Co(II) and Zn(II) metal organic frameworks. J. Catal. 385, 324–337.

Qian, J., Li, T., Hu, Y., Huang, S., 2017. A bimetallic carbide derived from a MOF precursor for increasing electrocatalytic oxygen evolution activity. Chem. Commun. 53, 13027–13030.

Wang, Y., Cao, H., Zheng, B., Zhou, R., Duan, J., 2018. Solvent- and pH-dependent formation of four zinc porous coordination polymers: framework isomerism and gas separation. Cryst. Growth Des. 18, 7674–7682.

Wang, J., Zhang, J., Jin, F., Luo, Y., Wang, S., Zhang, Z., Wu, Y., Liu, H., Lu, J.Y., Fang, M., 2015. Synthesis of an exceptional water-stable two-fold interpenetrated Zn(II)-paddlewheel metal–organic framework. CrystEngComm 17, 5906–5910.

Zhang, D., Wang, M.M., Jiang, N., Liu, Y., Yu, X.N., Zhang, H.B., 2020. Electrochemical corrosion behavior of Ni-doped ZnO thin film coated on low carbon steel substrate in 3.5% NaCl solution. Int. J. Electrochem. Sci. 15, 4117–4126.